Cetuximab-Conjugated Perfluorohexane/Gold Nanoparticles for Low Intensity Focused Ultrasound Diagnosis Ablation of Thyroid Cancer Treatment

Yue Ma
Harbin Medical University
Lingling Wang
Harbin Medical University
Haixia Li
Harbin Medical University
Wen Cheng
Harbin Medical University
Xiulan Zheng
Harbin Medical University
Ying Liu (liuying865@yahoo.com)
Harbin Medical University https://orcid.org/0000-0001-5106-650X

Research

Keywords:

Posted Date: June 5th, 2020

DOI: https://doi.org/10.21203/rs.3.rs-21316/v2

Version of Record: A version of this preprint was published at Science and Technology of Advanced Materials on January 31st, 2020. See the published version at https://doi.org/10.1080/14686996.2020.1855064.

Abstract

Chemotherapeutic efficacy plays a significant role in the development of nanotheranostic systems for drug delivery in tumor cells. In this study, we demonstrate the self-assembly of C225 conjugate, Perfluorohexane/Gold Nanoparticles (Au-PFH-NPs), which results in low-intensity focused ultrasound diagnosis ablation of thyroid cancer treatment. Cetuximab-Conjugated Perfluorohexane/Gold Nanoparticles (C-Au-PFH-NPs) showed excellent stability in water, PBS, and 20% rat serum. Transmission electron microscopy images revealed the effective construction of C-Au-PFH-NPs with commonly spherical assemblies. The incubation of C625 thyroid carcinoma with C-Au-PFH-NPs triggered apoptosis, which was confirmed by flow cytometry analysis. The C-Au-PFH-NPs showed remarkable antitumor efficacy in human thyroid carcinoma xenografts. The histopathological results additionally confirm the achieved outcomes. Furthermore, we successfully examined the efficiency of C-Au-PFH-NPs when using the thyroid carcinoma low-intensity focused ultrasound (LIFUS) diagnostic imaging in vivo. These findings are clear for LIFUS agents with high performing images. It is also identified that different therapeutic purposes will have extensive potential for future biomedical purposes.

1. Introduction

Anaplastic thyroid carcinoma (ATC) is one of the most malignantcarcinomas. It is comparatively rare, and is characterized by fastproliferation, neck invasion, and remote metastasis [1–4]. ATC'ssevere prognosis is due to the rapid progression of tumors beforediagnosis. Current treatment is based on different combinations ofchemotherapy, and exterior ray radiation has been unsuccessful inenhancing survival, resulting in an average survival rate of 4 to 6months and less than 20% survival rate in 12 months [5–8].Therefore, there are convincing arguments for the development of anew theranostic approach for initial finding and efficient ATCtreatment [9–11].

Recently, triggerable drug-charged nanocarriers coupled withmultiple internal or external stimuli, such as pH, temperature,ultrasound, laser, and microwave radiation, have been extensivelyexplored for personalized treatment to enable controlled release.They have shown an excellent possibility to deliver enhancedanticancer treatment impact, with decreased systemic toxicity[12–14]. Low-intensity concentrated ultrasound (LIFUS) has beenexhaustively researched for tumor treatment along with the use ofultrasound imaging analysis as a potential exterior activate, whichis noninvasive and displays significant tissue-penetratingcapacity. Particularly, it can significantly increase the efficacyof chemotherapy, avoiding harm to nearby cells, and reducingadversarial side effects [15]. However, the discharge ofLIFUS-triggered drugs from nanocarriers and further tumor therapyis still unsatisfactory. This is largely attributable to thecomparatively lower accumulation efficacy of nanoparticles-chargednano transporters at the tumor sites. Accordingly, numerousnanotransporters have been extensively examined to enhance theaggregation of a large number of tumors without causing any sideeffects [15–17].

Several reports have shown that overexpression of the epidermalgrowth factor receptor (EGFR) is strongly associated with tumorprogression, migration, and invasion. EGFR is common in ATCpatients [18].

Antibodies or small molecules based on EGFRimmunotherapy can significantly increase the therapeutic effectagainst ATC. A human, murine chimeric EGFR-targeted monoclonalantibody called cetuximab has shown high empathy in the human EGFRextracellular domain. It inhibits the signals of the epidermalgrowth factor in cells by delaying usual receptor functions[19–21]. The Food and Drug Administration (FDA) has approvedpreclinical treatments using cetuximab for the treatment of neckand head carcinoma and colorectal carcinoma with EGFR-expressingcancer tumors. This C225 might be a suitable objective for thestructure of nanocarriers to improve the outcome of ATC therapy.Remarkably, some researchers have revealed that for a wide spectrumof cancers, the blend of C225 with CPT-11 equivalents such asPerfluorohexane/Gold Nanoparticles (Au-PFH-NPs) has significantsynergetic antitumor effects [22–25], thus, enhancing ATCdiagnostics. However, owing to the reduced vascular dispersal ofC225 and the hydrophobicity of the Au-PFH-NPs, the nanoparticles'(NPs) penetrability in the growth and their quantity in the tumorarea were inherently imperfect, which greatly debilitated theiranticancer efficacy. Fortunately, these problems can be diminishedby incorporating Au-PFH-NPs and C225 into one nanotransporter toattain a C225 and Au-PFH-NP combination chemotherapy whilesimultaneously enabling the targeted capability for nanocarriers[26–29].

Furthermore, monitoring medical imaging is essential for earlydiagnosis and tumor progression. Numerous researchers have proposedthat LIFUS has the potential to achieve concurrent ultrasound (US)and medication transfer, meeting the present need of the initialtreatment and the ATC therapy [30–32]. Due to variability and hugedimensions of microbubbles to realize the tumor, the theranosticstrategy of conservative US agents, such as microbubbles,demonstrate outstanding imaging capability but are not appropriatefor drug delivery. To avoid this problem, we intensively studiedphase-changing NPs that could be activated via LIFUS.Phase-changing NPs provide important benefits in tumor theranosticsfor the supply of tumor US and US-triggered drugs [33–35]. This newstrategy offers the possibility of developing a treatment formalignancy and addressing the present theranostic needs,significantly contradicting ATC.

The objective of this study was to modify the C225 nanocarrierto targetedly prevent ATC that might accrue in cancer cells, inaddition to the enhanced permeability and retention (EPR) effect,through the tumor homing belongings of the C225. The Au-PFH-NPspayload release and the LIFUS-triggered synergistic chemotherapywith C225 potentially make the best use of therapeutic efficacy,improving USI, and diminishing the side effects of chemotherapy, asshown in **Figure 1**. Due to its tremendousbiodegradability and biocompatibility, we used a perfluorohexane(PHF core as the shell structure of the nanocarrier. We thensynthesized phase-changing NPs with PHF liquid (29°C boilingpoint). Meanwhile, the Au-PFH-NPs were burdened into the NPs whilethe C225 was conjugated on the surface of gold nanoparticles,affording (C-Au-PFH-NPs) C225-conjugated Au-PFH-NPs-charged phasetransformation. To our knowledge, this is the first work of aLIFUS-mediated C225 modified nanosystem that assimilates tumorstargeting both US imagery and US activated drug conveyance totackle ATC.

2. Experimental Section

The detailed experimental procedures are given in the supportinginformation.

2.1. Cell culture and nude mice

The Cell Bank of the Chinese Academy of Sciences (Shanghai,China) acquired a human anaplastic thyroid carcinoma line (C643).The cells were grown in medium RPMI-1640 containing 10% FBS and 1%penicillin-streptomycin at 37°C in humidified air with 5%CO_2. At the Laboratory Animal Center of Department ofUltrasound, Harbin Medical University Cancer Hospital (Harbin,China), BALB/C Female both mice and nude mice (balancing about 19g, 25 days) were bought then raised. All animals on our studieswere collected from the Harbin Medical University Cancer HospitalLaboratory Animal Center and retained in accordance with rulesauthorized by the Harbin Medical University's Animal EthicsCommittee (Harbin, China). Furthermore, all animal experimentalactivities were strictly in line with the policy of the HarbinMedical University's Institutional Animal Care and Use Committee(IACUC), and this study was endorsed by the IACUC.

In order to start an ATC model in nude mice, C643 cells werecollected, splashed thrice with the FBS free medium of RPMI-1640,and subcutaneously inoculated into each mouse's left flank (3× 10^7 C643 cells in 150 μL FBS freemedium of RPMI-1640 each mice). A Vernier caliper was used tomeasure the length and width of the tumour and the tumour quantitywas considered by the calculation: volume-(length aswidth× 2)/2.

2. *In vitro* analysis

2. 1. In vitro intracellularuptakeC-Au-PFH-NPs

In cultivation dishes, seeded the C643 cells for CLSM at a massof 1×10^6 cell mL/dish, grown at 37°C in moistened aircomprising 5% CO_2. The cells were spilt into four groupsafter 24 h of culture: C-Au-PFH-NPs were handled respectively with10 min and 15 min Dil- labeled C-Au-PFH-NPs (1mg/mL), and afterblocking the cells were washed three times with PBS. Then, Dil-labeled C-Au-PFH-NPs (1 mg/mL) incubated the cells. The cells werewashed with PBS three times after 2 h incubation withnanoparticles, fixed with 4 percent paraformaldehyde (200 μL) for15 minutes, and then gestated by DAPI (10 μg/mL, 200 μL) for 20min. Lastly, CLSM pictured the dishes [36–38].

2.2.3. In vitro cytotoxicity assay

The CCK-8 assay assessed the cell viability. C643 cells wereseeded into 96-well plates (1×10^3 cells per well,100μL). After 24- hours' incubation to assess the cell viabilityAu-PFH-NPs and C-Au-PFH-NPs treated at levels of 10, 5, 2.5, 1.25,0.625 and 0.312 μM for 24 hours. Au-PFH-NPs and C-Au-PFH-NPs cellswere incubated for 24 hours. The positive control used as theuntreated C643 cells. The in vitro cytoxicicty assay performed andthe calculated made by the company manufactures guidelines.

2.2.4. Apoptosis examinations

The cells were seeded (4×10^6 C643 cells per well, 1.5mL) into a 6-well dish and grown at 37°C in a humidified incubatorwith 5% CO_2 for 24 hours. The IC_{50}concentration used by Au-PFH-NPs and C-Au-PFH-NPs. The cellapoptosis assay grouping technique was in accordance with the cellviability assay group. After administering IC_{50}concentration of the formulations of Au-PFH-NPs and C-Au-PFH-NPswas implemented 2 hours later [39–41].

2.2.5. Cell cycle arrestexaminations

The cells were seeded (4×10^6 C643 cells per well, 1.5mL) into a 6-well dish and grown at 37°C in a humidified incubatorwith 5% CO_2 for 24 hours. The IC_{50}concentration used by Au-PFH-NPs and C-Au-PFH-NPs. The cells weregathered and analyzed in the PI-stained cells after 24 hours ofculture, and the percentages of the cells in the G0/G1, S phase,and G2/M phases were evaluated [42–44].

2.2.6. *In vitro* fluorescence imaging inxenografts tumour

A continuous dosage of DiR labeled Au-PFH-NPs and C-Au-PFH-NPs(2 mg/mL, 200μL) was given to C643 tumour-bearing mice. With 1%pentobarbital, all mice were totally narcotized and fluorescencepictures were acquired before injection and 3h, 6h and 24 hpost-injection. A vivid fluorescence imaging for tiny animalsevaluated the fluorescence intensity changes in the tumour areas*in vivo*. For *ex vivo* fluorescence imaging, thesignificant organs and tumour of one mouse were gathered. Inaddition, Dil-labeled Au-PFH-NPs and C-Au-PFH-NPs (2.5 mg per mL,150 μL) were injected through the intravenous of C643tumour-bearing mice were injected six hours after injection. At thepredetermined post-injection moment, tumour matters and significanttissues were gathered, segmented, and ice-covered. DAPI dyeing wasconducted in the dark for 5 min after fastening with 4%paraformaldehyde. The biodistribution of Dil-labeled Au-PFH-NPs andC-Au-PFH-NPs was monitored by CLSM [45–47].

2.2.7. Therapeutic efficacy of *invivo*

When the subcutaneous tumour reaches 100 mm^3 involume, an antitumour assay was conducted on xenografts of micecarrying anaplastic thyroid cancer. The tumour-bearing mice werearbitrarily split into 3 communities (n-5 per unit): control group(Saline) and free Au-PFH-NPs and C-Au-PFH-NPs were administered bythe organizations . Two hundred microliters of the blend wasinjected with the same dose of Au-PFH-NPs and C-Au-PFH-NPs (1mg/kg) through the tail vein in a 1% saline solution weredetermined six hours after injection with the US agent filling theinvestigation with the tumour superficial. Afterward theinoculations of C643 cells, 5 consecutive treatments were performedeach 72 hours starting on day 20 and ending on day 37. Each mouse'stumour dimensions and weight was recovered every three days, andchanges in tumour volume were examined from the relative tumourdimensions V/V_0 (V_0: initial volume prior totreatment), and tumour growth curves were drawn at the same time.On day 37 days, all mice were euthanized and dissected and weighedthe tumour masses. In addition, studies in histology andimmunohistochemistry were conducted. Sections of the tissue werestained with histophalogy [48–50].

3. Results And Discussion

3.1. Characterization of C-Au-PFH-NPs

Having these compounds at hand, we examined the transmissionelectron microscopy (TEM) analysis of Au-PFH-NPs (1 and 1a zoomview) and C-Au-PFH-NPs **(Figures 1** and**2).** Their ability to recapitulatethe self-assembly behavior in aqueous solutions was tested. Forthis purpose, we dissolved the C-Au-PFH-NPs prodrugs in dimethylsulfoxide (DMSO 10 mg/mL) and then rapidly injected them intodeionized (DI) water under ultrasonication. This procedure allowedus to validate that the solution was transparent and slightlybluish. Electron microscopy revealed that the drug moleculesself-assembled to form a spherical nanoparticle structure. Thedynamic light scattering (DLS) showed a single peak distribution ofthe nanoparticles. The average hydrodynamic diameter (intensity) ofthe compound 1 was ~107.1 nm, and compound 2 was ~108.0 nm(**Figure 2B**). There is, however, a certain adhesionbetween nanoparticles formed by the self-assembly of simplesmall-molecule drugs [51–53]. Therefore, we have a miscible liquidwith many hydrophobic drugs by combining the prodrug with theappropriate amount of C225 molecules. These nano-assemblies wereformed and widely used for in vivo drug delivery, to solve theproblem of adhesion and to optimize cancer-specific drug delivery.Then, we measured the stability of C-Au-PFH-NPs with variousparameters such as water, PBS, and 20% rat serum, which showed asignificantly stable size in various parameters (**Figure2C**). Although C-Au-PFH-NPs can self-assemble to formnanoparticles, taken together they may not be sufficiently stable.Therefore, C225 nanoparticles loaded with Au-PFH were investigatedfurther to evaluate their anticancer efficacy in vitro.

3.2. *In vitro* cell experiments

3.2.1. *In vitro* intracellularuptake

As illustrated in **Figure 3**, the much tougherred fluorescence derived from Dil-labeled C-Au-PFH-NPs was moreconcentrated in the C-Au-PFH-NPs group around the cytomembrane ofC643 cells compared to the non-target and antagonistic groups [54].Furthermore, larger quantities of red fluorescence were noted afterexposure to the C-Au-PFH-NPs group. These findings indicated thatdue to the elevated tumor-homing characteristics of C225, theC-Au-PFH-NPs could adhere to C643 cells, and considerablyencouraged intracellular uptake of the C643 cells. In theresentment group, the C-Au-PFH-NPs lost the capacity to target theC643 cells because of the congestion of surplus free C225, leadingto low levels of C-Au-PFH-NPs around the cells. This demonstratedthat the C-Au-PFH-NPs' desired targeting effectiveness was theoutcome of the EGFR-mediated directing capacity.

3.2.2. In vitro cytotoxicity assay

The cell counting kit -8 assay assessed the cell viability ofdifferent NP formulations at distinct levels, through adose-dependent model. As illustrated in Figure 4A, the cellviability of nanoparticles in the analyzed dose range was greaterthan 80% at 10 mg/mL. The comparatively small and insignificantviability proposed that the elevated biocompatibility ofphase-changing NPs was appropriate

for in vivo application.Reasonably, the cell viabilities of Au-PFH-NPs and C-Au-PFH-NPsdecreased considerably as levels of C-Au-PFH-NPs increased.Particularly, the cell viability of the cells treated withC-Au-PFH-NPs was low at the same concentration, implying that themixture of C-Au-PFH-NPs could boost cytotoxicity synergistically.Cell viability of C-Au-PFH-NPs. The remarkably improvedcytotoxicity of C-Au-PFH-NPs may be due to the increased cellmembrane permeability caused by the cavitation effect and theimproved cell viability of C-Au-PFH-NPs at the objective location,significantly increasing the inhibitory impression of C-Au-PFH-NPson cell development.

3.2.3. Cell apoptosis and cell cycle assays

Next, we evaluated cellular apoptosis. In several groups, totalapoptosis (TA) improved as follows: control and Au-PFH-NPs andC-Au-PFH-NPs, respectively (Figure 4B). It should be noted that theapoptosis proportion of Au-PFH-NPs was smaller than that ofC-Au-PFH-NPs, whereas it was significantly greater than that ofC-Au-PFH-NPs. Cell cycle assays were also conducted to evaluatewhether the cell cycle was influenced by the anti-proliferationused by Au-PFH-NPs and C-Au-PFH-NPs. Compared to the control group,a higher percentage of the G2/M phase was perceived in allpreserved sets (Figure 4C). The arrest cycle in the C-Au-PFH-NPsG2/M phase was higher than that in the control group but higherthan that in the C-Au-PFH-NPs, which is consistent with the resultsof cytotoxicity and the apoptosis assays mentioned above. Anenhanced proportion of the cell cycle in the G2/M phase wasdetected, and the distinct declaration stages were ascribed to thedistinct effects among distinct tumor cells. Hence, theC-Au-PFH-NPs showed an important cell cycle arrest in C643 cellsduring the G2/M phase impact.

Complete deliberation of the outcomes of the in vitro experimentindicated that nanoparticles could aid as exceptional vehicles forAu-PFH-NPs and C-Au-PFH-NPs. Their combination with C225 enabledthe targeted enhancement of cell recognition and endocytosis andenhanced the therapeutic effect of C-Au-PFH-NPs. Furthermore, wemaximized the cell proliferation inhibitory effects which may bedue to the increased cell membrane permeability caused bycavitation and ultrasound-targeted microbubble destruction (UTMD)effects improved the release of C-Au-PFH-NPs at the objective site,significantly increasing the inhibitory effect on proliferation ofthe tumor cells.

3.4. *In vivo* fluorescence imaging of xenografttumors

Fluorescence imaging was implemented at the pre-arranged periodopinions to assess the targeting effectiveness and biodistributionof Au-PFH-NPs and C-Au-PFH-NPs *in vitro*. Compared to thenon-targeted group's small fluorescence signal at each stage, thetargeted group's accumulating fluorescence signal seemed to bepresent at the tumor site and peaky at 6 hours at values six timesgreater than that of the control group (3.94±0.98), sometimes 109vs. (9.03±1.02) 108 (ps/cm^{-2}/sr)/(μW/cm),respectively, (**Figure 5A**). The intensity of thefluorescence removed the tumor. Significant tissues were examinedafter 24 h ex vivo. The tumor intensity fluorescence in theselected group was still two-times greater than that in thenon-target group, (2.99±0.38) sometimes 108 vs. (2.09±0.32) 108(ps/cm^{-2}/sr)/(μW/cm), respectively. There wasvirtually no distinction between the targeted and non-targetedgroups in the intensified

fluorescence in the corresponding bodies.Meanwhile, considerably greater red fluorescence signals were notedin the targeted group's tumor cryosections at 6 h under CLSMfollowing the tumor tissue's ultrathin segment, relative to thefewer red signals in the non-target group. It should be noted thatthe red fluorescence signals in the tumor cryosections of theAu-PFH-NPs group were significantly better compared to those of theC-Au-PFH-NPs group after irradiation. The distribution of thefluorescence signal in the main organs showed no significantalteration in either group, except in the liver and spleen (Figure5B and C). The non-targeted group's low fluorescence signals at thetumor site may have resulted from the EPR effect, which facilitatedinert combination in tumor tissues. Contrastingly, the improvedfluorescence signal of the target group was primarily due to theC225-mediated endocytosis mechanism. Additionally, the C-Au-PFH-NPscould overcome the biological barriers of the tumor. Theaccumulation of C-Au-PFH-NPs at the objective places was endorsedafter microbubble oscillation, cavitation, and destruction. Duringthe process of the oscillation and crash of the acousticmicrobubble by the US-targeted microbubble removal impact, the cellmembrane could be interrupted, and it's permeability was enhanced,allowing the greater accumulation of C-Au-PFH-NPs at the objectivelocations. These conclusions further confirm that C225 has thepotential to precisely carry nanocarriers to tumor cells,preventing them from rapidly reentering into the systemiccirculation, allowing extravascular diagnosis and efficientantitumor therapy with an agent.

3.3.7. *In vitro* ultrasound imaging

Based on the targeted accumulation capacity of Au-PFH-NPs andC-Au-PFH-NPs in tumor cells, we explored the potential ofphase-changing nanoparticles to aid as US contrast to improve USland treatment scratches [55–57]. Following the administration ofvarious medicines before LIFUS irradiation, even lower or anechoiccontrast improved US signals were observed in each group(**Figure 6A**). LIFUS was performed in all groups 6 hafter the administration of various treatments, at the same timeperiods with in vivo ultrasound imaging. Expressively sturdierspot-like echo signs slowly accrued in both modes at the tumorplaces in the treated group, while no evident deviations weredetected in the saline group, and only negligible signs appeared inthe non-target group. This suggested that C225 eased the directionof the tumor tissue accretion. Large quantities of microbubbleswere produced when phase-changing NPs were subjected to ADV at theLIFUS-triggered tumor site, resulting in improved US imaging.However, owing to the absence of C225-mediated targeting capacity,the inadequate ADV of the Au-PFH-NPs and C-Au-PFH-NPs could noteffectively improve ultrasound imaging. Furthermore, no obviousenrichment was observed without the LIFUS irradiation in theAu-PFH-NPs, and the C-Au-PFH-NPs alone could not improve theultrasound imaging *in vitro,* shown in Figure 6B-D. Thesefindings highlighted that C-Au-PFH-NPs were appropriate asultrasound imaging agents and efficient as *in vivo*nanocarriers because of their relative stability. This is in linewith the outcomes of the ultrasonic imaging, additionally verifyingthe effectiveness of the beleaguered ultrasonic of C-Au-PFH-NPslower than that of the potential of LIFUS irradiation and localLIFUS radioactivity to boost the precision of phase-changingC-Au-PFH-NPs.

3.3.8. Therapeutic efficacy *invivo*

The antitumor efficacy *in vivo* was explored in thesubcutaneous C643 models, to assess the therapeutic efficacy of themixture of Au-PFH-NPs and C-Au-PFH-NPs *in vitro*. Numerouspictures of separate groups of mice were drawn to demonstrate theimpact of the therapy. (**Figure 7A-C**). Thetherapeutic effectiveness was evaluated by tracking changes in eachgroup's tumor volume. It was observed that the tumor in the salinegroups was debauched, and there was no significant decrease in thetumor dimensions in the C-Au-PFH-NPs group, indicating that itsdose was dependable *in vivo,* and that thewell-known epidermal growth factor was a target for tumor cellidentification and treatment. However, the C-Au-PFH-NP accumulationat the tumor site depended solely on the existence of vesselfenestration and vascular leakage, and the inadequate drug releaseat the tumor site restricted the therapeutic effect. These findingsshowed that the C-Au-PFH-NPs in nude mice could enhance thetherapeutic effect of anaplastic subcutaneous thyroid cancer.Additionally, compared with the control (saline) groups, H&E,procaspase 9 (brown), and cleaved-caspase 3 (brown) expressionlevels were enhanced. The Ki67 staining and TUNEL assay were usedto measure the apoptosis of the tumor *in vivo* (Figure 7D).Furthermore, while Au-PFH-NPs significantly reduced body weightduring the course of the therapy, the use of C-Au-PFH-NPs showed nostatistically significant impact on the body weight among all micegroups.

The above findings clearly highlight that the combination ofC-Au-PFH-NPs attained a notable excellent therapeutic effect tocounter ATC in nude mice, highlighting the importance of thesecurity of beleaguered tumor treatment. This diagnostic approachis preferred for ATC, significantly improving the healing capacity,without noticeable side effects.

4. Conclusion

The data presented in this study highlight a strategic rationalefor the effectiveness and safety of Au-PFA-NPs. As the syntheticAu-PFA-NPs and C-Au-PFA-NPs are fully biocompatible composites withminimal modifications, the safety risks can be minimized byconsidering their clinical translation. Furthermore, consideringthe ability of Au-PFA-NPs to overcome the cetuximab (C225)-conjugated C-Au-PFA-NPs, it was expected that this approach couldbe an optional therapeutic platform to treat patients withdrug-resistant cancer. Lastly, we envision that in addition totaxane agents, this C-Au-PFA-NPs-based approach could be a simpleyet broadly applicable strategy to improve tolerance and present abetter organized cytotoxic nanotherapeutic approach compared toother antitumor agents.

Declarations

Acknowledgements

None

Authors' contributions

Y.M. and L.W. assisted with NP synthesis and characterization;H. L. assisted with molecular and biochemical analysis; W.C. andX.Z. - assisted with data curation, formal analysis, andvalidation; Y.L.

assisted with supervised the research.

Funding

None

Availability of data and materials

All data and material are included in the article and itsadditional files.

Ethics approval and consent to participate

All animal experiments were approved by the Ethics Committee ofthe Harbin Medical University Cancer Hospital in accordance withthe guidelines on animal care and use (File No: 2018-3).

Consent for publication

Not applicable.

Competing interests

The authors declare that they have no competing interests.

References

[1] C. Valkenborgh, L. Médart, L. Collignon, Muscle Metastasisfrom Undifferentiated (Anaplastic) Thyroid Carcinoma, Journal ofthe Belgian Society of Radiology. 103 (2019) 27.doi:10.5334/jbsr.1604.

[2] H. Yamazaki, H. Iwasaki, N. Suganuma, S. Toda, K. Masudo, H.Nakayama, Y. Rino, M. Masuda, Anaplastic thyroid carcinomadiagnosed after treatment of lenvatinib for papillary thyroidcarcinoma, Endocrinology, Diabetes & Metabolism Case Reports. 2019(2019). doi:10.1530/EDM-19-0085.

[3] D. Shelly, D. Gupta, S. Mishra, R. Bharadwaj, Osteoclasticvariant of anaplastic thyroid carcinoma: A case report of rareentity., Journal of Cancer Research and Therapeutics. 15 (2019)704–707. doi:10.4103/jcrt.jcrt_355_16.

[4] E. Spartalis, D.I. Athanasiadis, D. Chrysikos, M. Spartalis,G. Boutzios, D. Schizas, N. Garmpis, C. Damaskos, S.A. Paschou, A.Ioannidis, G. Tsourouflis, D. Dimitroulis, N.I. Nikiteas, HistoneDeacetylase Inhibitors and Anaplastic Thyroid Carcinoma, AnticancerResearch. 39 (2019) 1119–1127. doi:10.21873/anticanres.13220.

[5] L. Gou, H. Zou, B. Li, Long noncoding RNA MALAT1 knockdowninhibits progression of anaplastic thyroid carcinoma by regulatingmiR-200a-3p/FOXA1, Cancer Biology & Therapy. 20 (2019) 1355–1365.doi:10.1080/15384047.2019.1617567.

[6] J.-Y. Kim, H.Y. Youn, J. Choi, S.K. Baek, S.Y. Kwon, B.K.Eun, J.-Y. Park, K.H. Oh, Anoctamin-1 affects the migration andinvasion of anaplastic thyroid carcinoma cells, Animal Cells andSystems. 23 (2019) 294–301. doi:10.1080/19768354.2019.1614981.

[7] Z. Pan, L. Li, Q. Fang, Y. Qian, Y. Zhang, J. Zhu, M. Ge, P.Huang, Integrated Bioinformatics Analysis of Master Regulators inAnaplastic Thyroid Carcinoma, BioMed Research International. 2019(2019) 9734576. doi:10.1155/2019/9734576.

[8] R. Eshraghi, G.A. Barkan, S.E. Pambuccian, Rhabdoid cells inthe fine needle aspirate of a neck mass in a patient with historyof melanoma: Anaplastic thyroid carcinoma, DiagnosticCytopathology. 47 (2019) 1232–1236. doi:10.1002/dc.24284.

[9] C. Jiao, L. Li, P. Zhang, L. Zhang, K. Li, R. Fang, L. Yuan,K. Shi, L. Pan, Q. Guo, X. Gao, G. Chen, S. Xu, Q. Wang, D. Zuo, W.Wu, S. Qiao, X. Wang, R. Moses, J. Xiao, L. Li, Y. Dang, X. Li,REGγ ablation impedes dedifferentiation of anaplastic thyroidcarcinoma and accentuates radio-therapeutic response by regulatingthe Smad7-TGF-β pathway, Cell Death and Differentiation. (2019).doi:10.1038/s41418-019-0367-9.

[10] A.A.L. Chavez, P. Iyer, I.M. Cazacu, M.E. Cabanillas, A.Rashid, M.S. Bhutani, Anaplastic Thyroid Carcinoma with GastricMetastasis, Current Health Sciences Journal. 44 (2018) 294–298.doi:10.12865/CHSJ.44.03.14.

[11] Z. Li, Y. Zhang, R. Wang, K. Zou, L. Zou, Geneticalterations in anaplastic thyroid carcinoma and targeted therapies,Experimental and Therapeutic Medicine. 18 (2019) 2369–2377.doi:10.3892/etm.2019.7869.

[12] A. Fomenko, A.M. Lozano, Neuromodulation and ablation withfocused ultrasound - toward the future of noninvasive braintherapy, Neural Regeneration Research. 14 (2019) 1509–1510.doi:10.4103/1673-5374.255961.

[13] T. Lemaire, E. Neufeld, N. Kuster, S. Micera, Understandingultrasound neuromodulation using a computationally efficient andinterpretable model of intramembrane cavitation, Journal of NeuralEngineering. 16 (2019) 46007. doi:10.1088/1741-2552/ab1685.

[14] Z. Liu, H. Ran, Z. Wang, S. Zhou, Y. Wang, Targeted andpH-facilitated theranostic of orthotopic gastric cancer viaphase-transformation doxorubicin-encapsulated nanoparticlesenhanced by low-intensity focused ultrasound (LIFU) with reducedside effect, International Journal of Nanomedicine. 14 (2019)7627–7642. doi:10.2147/IJN.S212888.

[15] A. Fomenko, C. Neudorfer, R.F. Dallapiazza, S.K. Kalia,A.M. Lozano, Low-intensity ultrasound neuromodulation: An overviewof mechanisms and emerging human applications, Brain Stimulation.11 (2018) 1209–1217. doi:10.1016/j.brs.2018.08.013.

[16] K. Schindler, R. Wiest, M. Kollar, F. Donati, EEG analysiswith simulated neuronal cell models helps to detect pre-seizurechanges, Clinical Neurophysiology : Official Journal of theInternational Federation of Clinical Neurophysiology. 113 (2002)604–614. doi:10.1016/s1388-2457(02)00032-9.

[17] K. Schindler, R. Wiest, M. Kollar, F. Donati, Usingsimulated neuronal cell models for detection of epileptic seizuresin foramen ovale and scalp EEG, Clinical Neurophysiology : OfficialJournal of the International Federation of ClinicalNeurophysiology. 112 (2001) 1006–1017.doi:10.1016/s1388-2457(01)00522-3.

[18] J. Simões-Pereira, R. Capitão, E. Limbert, V. Leite,Anaplastic Thyroid Cancer: Clinical Picture of the Last Two Decadesat a Single Oncology Referral Centre and Novel Therapeutic Options,Cancers. 11 (2019). doi:10.3390/cancers11081188.

[19] J. Ljubas, T. Ovesen, M. Rusan, A Systematic Review ofPhase II Targeted Therapy Clinical Trials in Anaplastic ThyroidCancer, Cancers. 11 (2019). doi:10.3390/cancers11070943.

[20] J. Jin, X. Wu, J. Yin, M. Li, J. Shen, J. Li, Y. Zhao, Q.Zhao, J. Wu, Q. Wen, C.H. Cho, T. Yi, Z. Xiao, L. Qu,Identification of Genetic Mutations in Cancer: Challenge andOpportunity in the New Era of Targeted Therapy, Frontiers inOncology. 9 (2019) 263. doi:10.3389/fonc.2019.00263.

[21] C. Garcia, C. Buffet, L. El Khattabi, M. Rizk-Rabin, K.Perlemoine, B. Ragazzon, J. Bertherat, F. Cormier, L. Groussin, METoverexpression and activation favors invasiveness in a model ofanaplastic thyroid cancer, Oncotarget. 10 (2019) 2320–2334.doi:10.18632/oncotarget.26798.

[22] W. Qiu, C. Zhang, S. Wang, X. Yu, Q. Wang, D. Zeng, P. Du,J. Ma, Y. Zheng, B. Pang, Y. Yu, F. Long, X. Pang, Z. Sun, A NovelAnti-EGFR mAb Ame55 with Lower Toxicity and Better Efficacy thanCetuximab When Combined with Irinotecan, Journal of ImmunologyResearch. 2019 (2019) 3017360. doi:10.1155/2019/3017360.

[23] Y. Zhu, J. Li, F. Jing, T. Ji, X. Guo, J. Yang, S. Jiao,Evaluation of the immune factors in the tumor environment beforeand after the treatment of cetuximab combined with chemotherapy,World Journal of Surgical Oncology. 11 (2013) 226.doi:10.1186/1477-7819-11-226.

[24] B. Cáceres, A. Ramirez, E. Carrillo, G. Jimenez, C.Griñán-Lisón, E. López-Ruiz, Y. Jiménez-Martínez, J.A. Marchal, H.Boulaiz, Deciphering the Mechanism of Action Involved in EnhancedSuicide Gene Colon Cancer Cell Killer Effect Mediated by Gef andApoptin, Cancers. 11 (2019). doi:10.3390/cancers11020264.

[25] K.E. Boyle, Z.W. Patinkin, A.L.B. Shapiro, C. Bader, L.Vanderlinden, K. Kechris, R.C. Janssen, R.J. Ford, B.K. Smith, G.R.Steinberg, E.J. Davidson, I. V Yang, D. Dabelea, J.E. Friedman,Maternal obesity alters fatty acid oxidation, AMPK activity, andassociated DNA methylation in mesenchymal stem cells from humaninfants, Molecular Metabolism. 6 (2017) 1503–1516.doi:10.1016/j.molmet.2017.08.012.

[26] F. Wang, M. Porter, A. Konstantopoulos, P. Zhang, H. Cui,Preclinical development of drug delivery systems forpaclitaxel-based cancer chemotherapy, Journal of ControlledRelease : Official Journal of the Controlled Release Society. 267(2017) 100–118. doi:10.1016/j.jconrel.2017.09.026.

[27] M.C. Prewett, A.T. Hooper, R. Bassi, L.M. Ellis, H.W.Waksal, D.J. Hicklin, Enhanced antitumor activity of anti-epidermalgrowth factor receptor monoclonal antibody IMC-C225 in combinationwith irinotecan (CPT-11) against human colorectal tumor xenografts,Clinical Cancer Research : An Official Journal of the AmericanAssociation for Cancer Research. 8 (2002) 994–1003.http://europepmc.org/abstract/MED/12006511.

[28] N.A. Zaidman, A. Panoskaltsis-Mortari, S.M. O'Grady,Differentiation of human bronchial epithelial cells: role ofhydrocortisone in development of ion transport pathways involved inmucociliary clearance, American Journal of Physiology. CellPhysiology. 311 (2016) C225-36. doi:10.1152/ajpcell.00073.2016.

[29] C.-Q. Huang, Y. Min, S.-Y. Wang, X.-J. Yang, Y. Liu, B.Xiong, Y. Yonemura, Y. Li, Cytoreductive surgery plus hyperthermicintraperitoneal chemotherapy improves survival for peritonealcarcinomatosis from colorectal cancer: a systematic review andmeta-analysis of current evidence, Oncotarget. 8 (2017)55657–55683. doi:10.18632/oncotarget.17497.

[30] S. Ishihara, N. Onoda, S. Noda, Y. Asano, Y. Tauchi, T.Morisaki, S. Kashiwagi, T. Takashima, M. Ohira, Sorafenib inhibitsvascular endothelial cell proliferation stimulated by anaplasticthyroid cancer cells regardless of BRAF mutation status,International Journal of Oncology. 55 (2019) 1069–1076.doi:10.3892/ijo.2019.4881.

[31] J.R. Wang, M.E. Zafereo, R. Dadu, R. Ferrarotto, N.L.Busaidy, C. Lu, S. Ahmed, M.K. Gule-Monroe, M.D. Williams, E.M.Sturgis, R.P. Goepfert, N.D. Gross, S.Y. Lai, G.B. Gunn, J. Phan,D.I. Rosenthal, C.D. Fuller, W.H. Morrison, P. Iyer, M.E.Cabanillas, Complete Surgical Resection Following NeoadjuvantDabrafenib Plus Trametinib in BRAFV600E-Mutated Anaplastic ThyroidCarcinoma, Thyroid : Official Journal of the American ThyroidAssociation. 29 (2019) 1036–1043. doi:10.1089/thy.2019.0133.

[32] K.L. Corrigan, H. Williamson, D. Elliott Range, D.Niedzwiecki, D.M. Brizel, Y.M. Mowery, Treatment Outcomes inAnaplastic Thyroid Cancer, Journal of Thyroid Research. 2019 (2019)8218949. doi:10.1155/2019/8218949.

[33] J.W. Bi, Y.L. Zou, J.T. Qian, W. Bin Chen, MiR-599 serves asuppressive role in anaplastic thyroid cancer by activating theT-cell intracellular antigen, Experimental and TherapeuticMedicine. 18 (2019) 2413–2420. doi:10.3892/etm.2019.7864.

[34] X. Wu, A. Benov, D.N. Darlington, J.D. Keesee, B. Liu, A.P.Cap, Effect of tranexamic acid administration on acute traumaticcoagulopathy in rats with polytrauma and hemorrhage, PloS One. 14(2019) e0223406. doi:10.1371/journal.pone.0223406.

[35] E.R. McGonagle, C. Nucera, Clonal Reconstruction of ThyroidCancer: An Essential Strategy for Preventing Resistance toUltra-Precision Therapy, Frontiers in Endocrinology. 10 (2019) 468.doi:10.3389/fendo.2019.00468.

[36] C.K. Song, S.H. Jung, D.-D. Kim, K.-S. Jeong, B.C. Shin, H.Seong, Disaccharide-modified liposomes and their in vitrointracellular uptake, International Journal of Pharmaceutics. 380(2009) 161–169. doi:10.1016/j.ijpharm.2009.07.014.

[37] M. Lei, G. Ma, S. Sha, X. Wang, H. Feng, Y. Zhu, X. Du,Dual-functionalized liposome by co-delivery of paclitaxel withsorafenib for synergistic antitumor efficacy and reversion ofmultidrug resistance, Drug Delivery. 26 (2019) 262–272.doi:10.1080/10717544.2019.1580797.

[38] Y. Wang, Y. Yang, Y. Yu, J. Li, W. Pan, X. Yang, Z. Zhang,S. Jiang, X. Yang, X. Wang, Transferrin Modified Dioscin LoadedPEGylated Liposomes: Characterization and In Vitro AntitumorEffect, Journal of Nanoscience and Nanotechnology. 20 (2020)1321–1331. doi:10.1166/jnn.2020.16955.

[39] M.S. Mohamed Kasim, S. Sundar, R. Rengan, Synthesis andstructure of new binuclear ruthenium(II) arene benzilbis(benzoylhydrazone) complexes: Investigation on antiproliferativeactivity and apoptosis induction, Inorganic Chemistry Frontiers. 5(2018) 585–596. doi:10.1039/c7qi00761b.

[40] M.K. Mohamed Subarkhan, L. Ren, B. Xie, C. Chen, Y. Wang,H. Wang, Novel tetranuclear ruthenium(II) arene complexes showingpotent cytotoxic and antimetastatic activity as well as lowtoxicity in vivo, European Journal of Medicinal Chemistry. 179(2019) 246–256.doi:https://doi.org/10.1016/j.ejmech.2019.06.061.

[41] M.K. Mohamed Subarkhan, R. Ramesh, Y. Liu, Synthesis andmolecular structure of arene ruthenium(ii) benzhydrazone complexes:impact of substitution at the chelating ligand and arene moiety onantiproliferative activity, New Journal of Chemistry. 40 (2016)9813–9823. doi:10.1039/C6NJ01936F.

[42] X.-L. Pang, G. He, Y.-B. Liu, Y. Wang, B. Zhang,Endoplasmic reticulum stress sensitizes human esophageal cancercell to radiation, World Journal of Gastroenterology. 19 (2013)1736–1748. doi:10.3748/wjg.v19.i11.1736.

[43] V. Ramalingam, S. Revathidevi, T. Shanmuganayagam, L.Muthulakshmi, R. Rajaram, Biogenic gold nanoparticles induce cellcycle arrest through oxidative stress and sensitize mitochondrialmembranes in A549 lung cancer cells, RSC Advances. 6 (2016)20598–20608. doi:10.1039/C5RA26781A.

[44] C. Huang, Y. Sun, M. Shen, X. Zhang, P. Gao, Y. Duan,Altered Cell Cycle Arrest by Multifunctional Drug-LoadedEnzymatically-Triggered Nanoparticles, ACS Applied Materials &Interfaces. 8 (2016) 1360–1370. doi:10.1021/acsami.5b10241.

[45] B.L. Allen-Petersen, R.C. Sears, Mission Possible: Advancesin MYC Therapeutic Targeting in Cancer, BioDrugs : ClinicalImmunotherapeutics, Biopharmaceuticals and Gene Therapy. 33 (2019)539–553.

doi:10.1007/s40259-019-00370-5.

[46] M. Li, Y. Ning, J. Chen, X. Duan, N. Song, D. Ding, X. Su,Z. Yu, Proline Isomerization-Regulated TumorMicroenvironment-Adaptable Self-Assembly of Peptides for EnhancedTherapeutic Efficacy, Nano Letters. (2019).doi:10.1021/acs.nanolett.9b03136.

[47] C. Scottà, G. Fanelli, S.J. Hoong, M. Romano, E.N.Lamperti, M. Sukthankar, G. Guggino, H. Fazekasova, K. Ratnasothy,P.D. Becker, B. Afzali, R.I. Lechler, G. Lombardi, Impact ofimmunosuppressive drugs on the therapeutic efficacy of ex vivoexpanded human regulatory T cells, Haematologica. 101 (2016)91–100. doi:10.3324/haematol.2015.128934.

[48] R. Bharadwaj, B.P. Sahu, J. Haloi, D. Laloo, P. Barooah, C.Keppen, M. Deka, S. Medhi, Combinatorial therapeutic approach fortreatment of oral squamous cell carcinoma, Artificial Cells,Nanomedicine, and Biotechnology. 47 (2019) 572–585.doi:10.1080/21691401.2019.1573176.

[49] X. Chen, W. Wu, S. Wang, J. Zhong, N.M. Djama, G. Wei, Y.Lai, X. Si, S. Cao, W. Liao, Y. Liao, H. Li, J. Bin, MagneticTargeting Improves the Therapeutic Efficacy of Microbubble-MediatedObstructive Thrombus Sonothrombolysis, Thrombosis and Haemostasis.(2019). doi:10.1055/s-0039-1695767.

[50] M.A. Vakilinezhad, A. Amini, T. Dara, S. Alipour,Methotrexate and Curcumin co-encapsulated PLGA nanoparticles as apotential breast cancer therapeutic system: In vitro and in vivoevaluation, Colloids and Surfaces. B, Biointerfaces. 184 (2019)110515. doi:10.1016/j.colsurfb.2019.110515.

[51] V. Gies, S. Zou, Systematic toxicity investigation ofgraphene oxide: evaluation of assay selection, cell type, exposureperiod and flake size, Toxicology Research. 7 (2018) 93–101.doi:10.1039/c7tx00278e.

[52] A. Bathla, R.A. Rather, T. Poonia, B. Pal, MorphologyDependent Photocatalytic Activity of CuO/CuO-TiO□ Nanocatalyst forDegradation of Methyl Orange Under Sunlight, Journal of Nanoscienceand Nanotechnology. 20 (2020) 3123–3130.doi:10.1166/jnn.2020.17397.

[53] A.Y. Xu, M.M. Castellanos, K. Mattison, S. Krueger, J.E.Curtis, Studying Excipient Modulated Physical Stability andViscosity of Monoclonal Antibody Formulations Using Small-AngleScattering, Molecular Pharmaceutics. 16 (2019) 4319–4338.doi:10.1021/acs.molpharmaceut.9b00687.

[54] Z. Cui, X. Zhang, X. Zhang, S. He, W. Gao, B. He, X. Wang,H. Zhang, Z. Zhong, Q. Zhang, Visualizing in vitro-in vivocorrelation of miktoarm copolymer nanomicelles in cancer cellularuptake and trafficking, (2019). doi:10.1101/755595.

[55] Y. Chen, Y. Liang, P. Jiang, F. Li, B. Yu, F. Yan,Lipid-PLGA hybrid microbubbles as a versatile platform fornon-invasive image-guided targeted drug delivery, ACS AppliedMaterials & Interfaces. (2019). doi:10.1021/acsami.9b10188.

[56] Y. Liu, S. Chen, J. Sun, S. Zhu, C. Chen, W. Xie, J. Zheng,Y. Zhu, L. Xiao, L. Hao, Z. Wang, S. Chang, Folate-Targeted andOxygen/Indocyanine Green-Loaded Lipid Nanoparticles for Dual-ModeImaging and

Photo-sonodynamic/Photothermal Therapy of OvarianCancer in Vitro and in Vivo, Molecular Pharmaceutics. 16 (2019)4104–4120. doi:10.1021/acs.molpharmaceut.9b00339.

[57] H. Yang, W. Cai, W. Lv, P. Zhao, Y. Shen, L. Zhang, B. Ma,L. Yuan, Y. Duan, K. Yao, A new strategy for accurate targeteddiagnosis and treatment of cutaneous malignant melanoma: dual-modephase-change lipid nanodroplets as ultrasound contrast agents,International Journal of Nanomedicine. 14 (2019) 7079–7093.doi:10.2147/IJN.S207419.

Figures

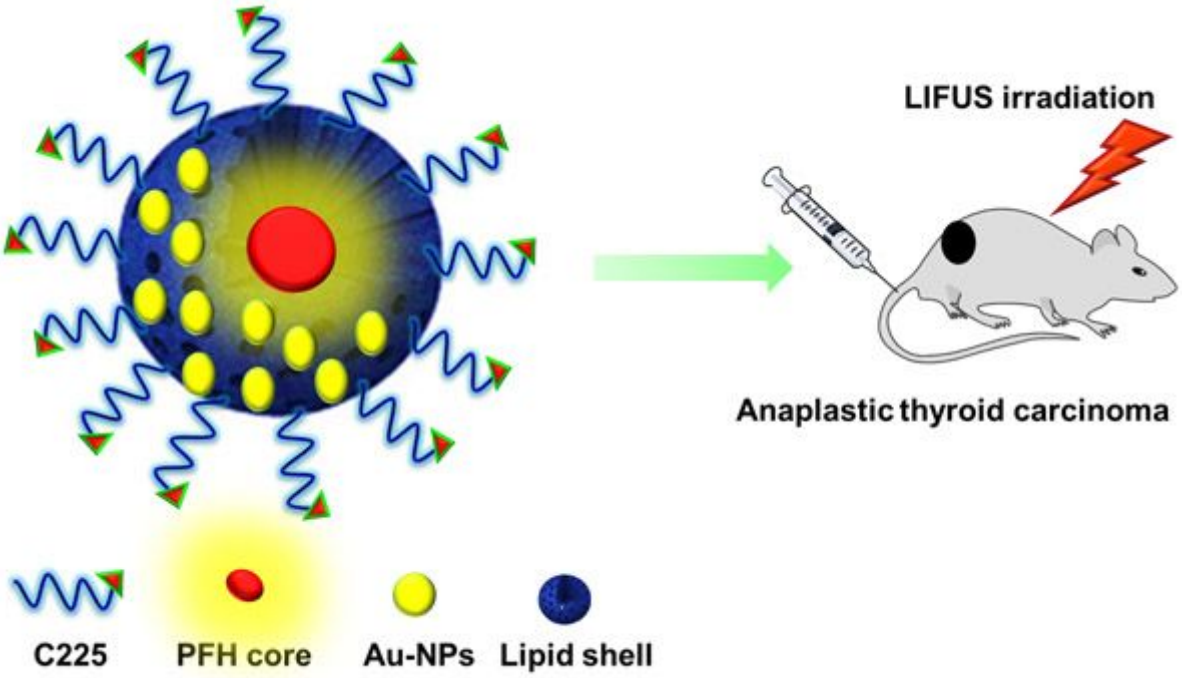

Figure 1

Design and NP formulation of C225 conjugates Au-PFH-NPs for safe and efficient in-vivo drug delivery.

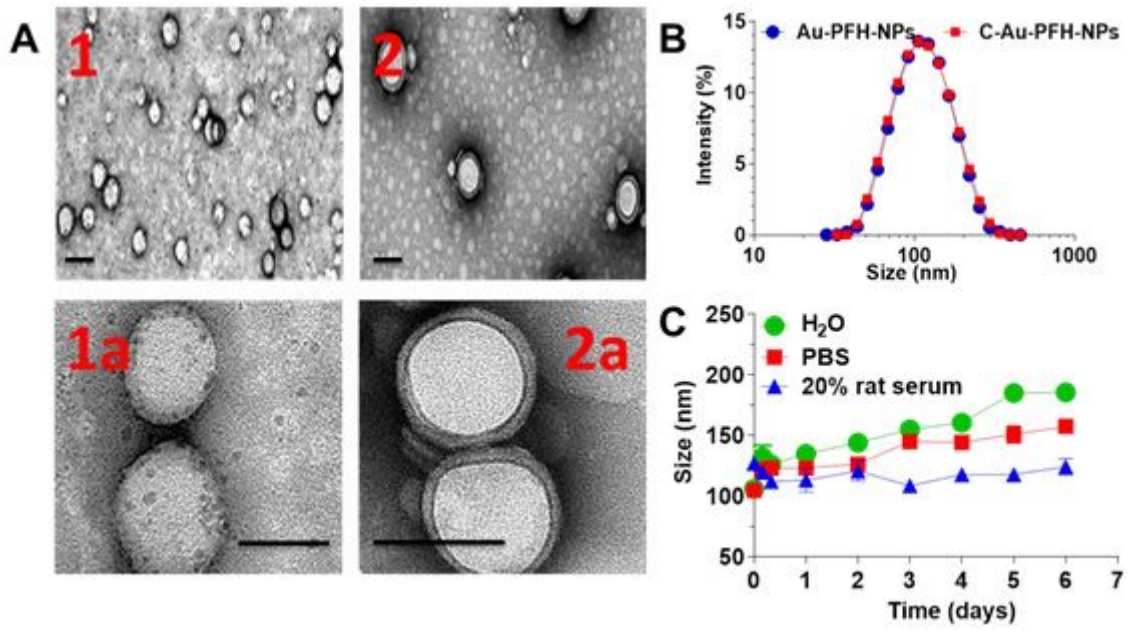

Figure 2

Analysis of Au-PFH-NPs and C-Au-PFH-NPs (A) TEM image of Au-PFH-NPs (1 and 1a zoom view) and C-Au-PFH-NPs (2 and 2a zoom view). Scale bars, 100 nm. (B) DLS image of Au-PFH-NPs and C-Au-PFH-NPs. (C) Stability of the Au-PFH-NPs and C-Au-PFH-NPs. in 50% water, PBS, and 20% rat serum at 37 °C.

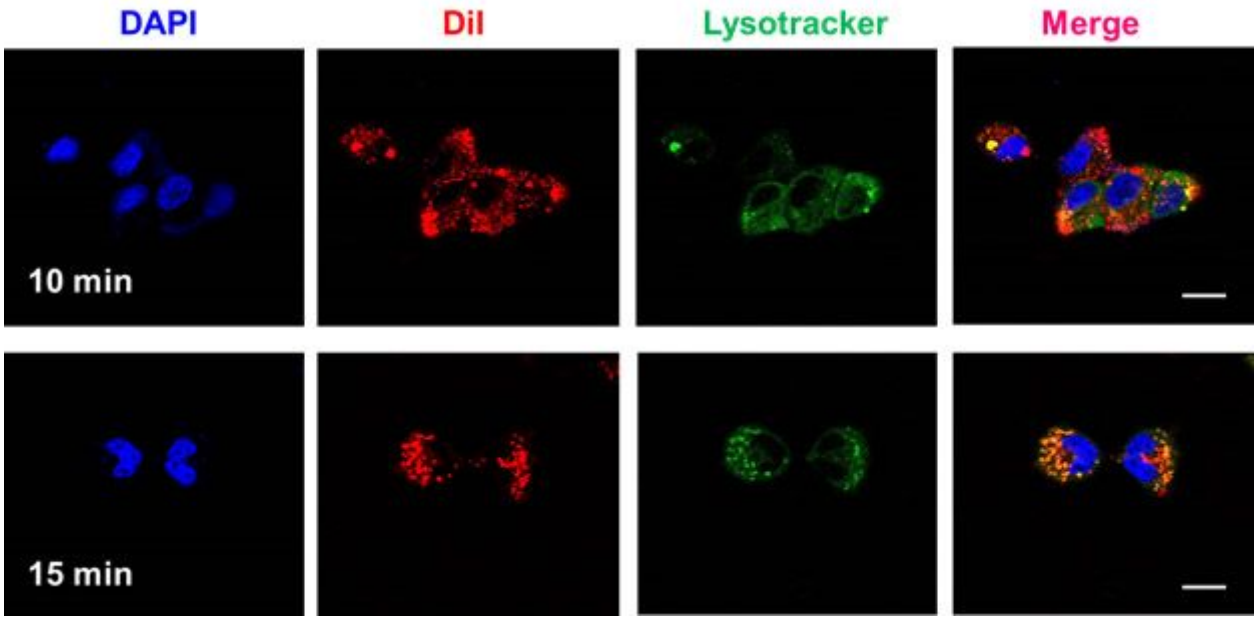

Figure 3

Cellular uptake of C-Au-PFH-NPs at 10 min and 15 min intervals.

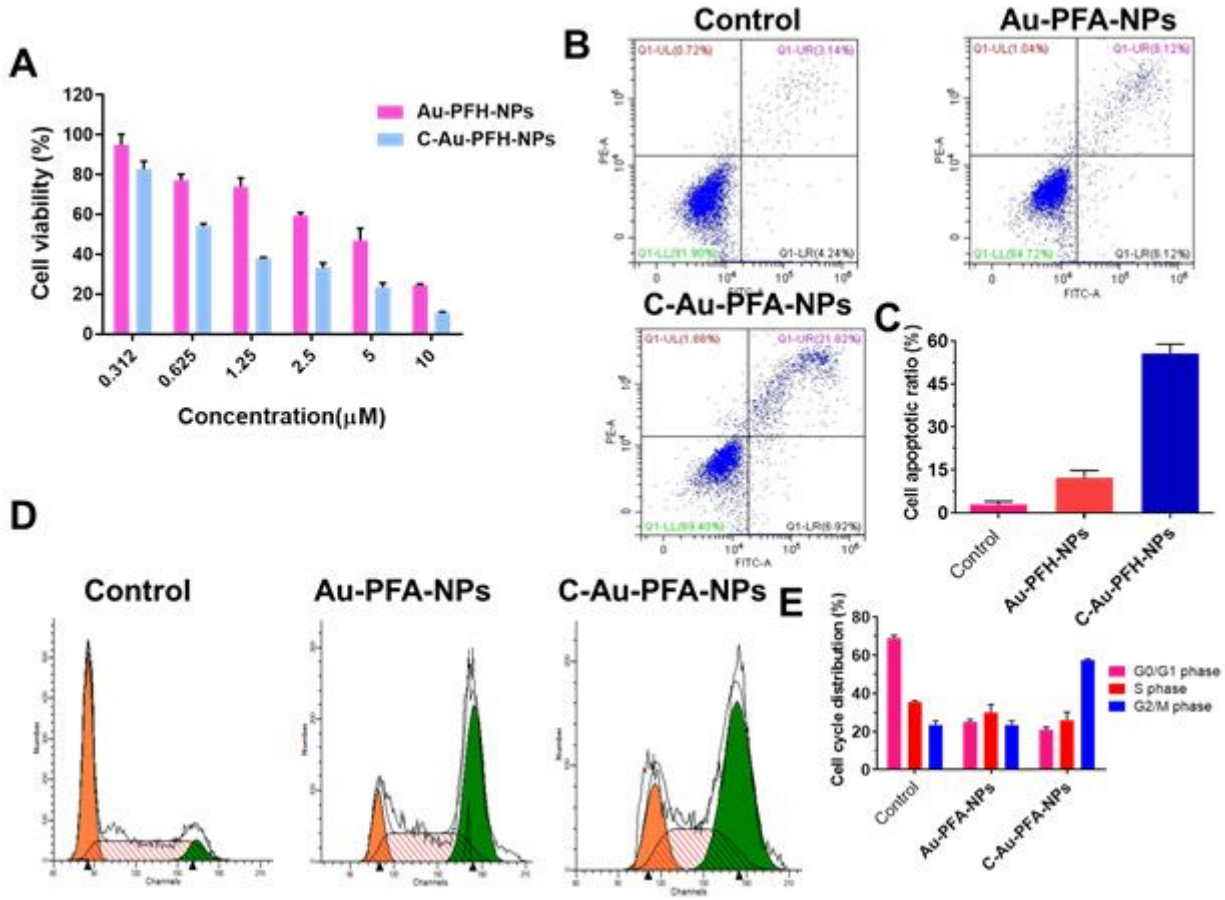

Figure 4

(A) In vitro cytotoxicity against C643 thyroid carcinoma cells. (B) Flow cytometry analysis of Au-PFH-NPs and C-Au-PFH-NPs. (C) Apoptosis quantification by flow cytometry analysis. (D) Cell cycle arrest of Au-PFH-NPs and C-Au-PFH-NPs. (E) Quantification of cell cycle arrest.

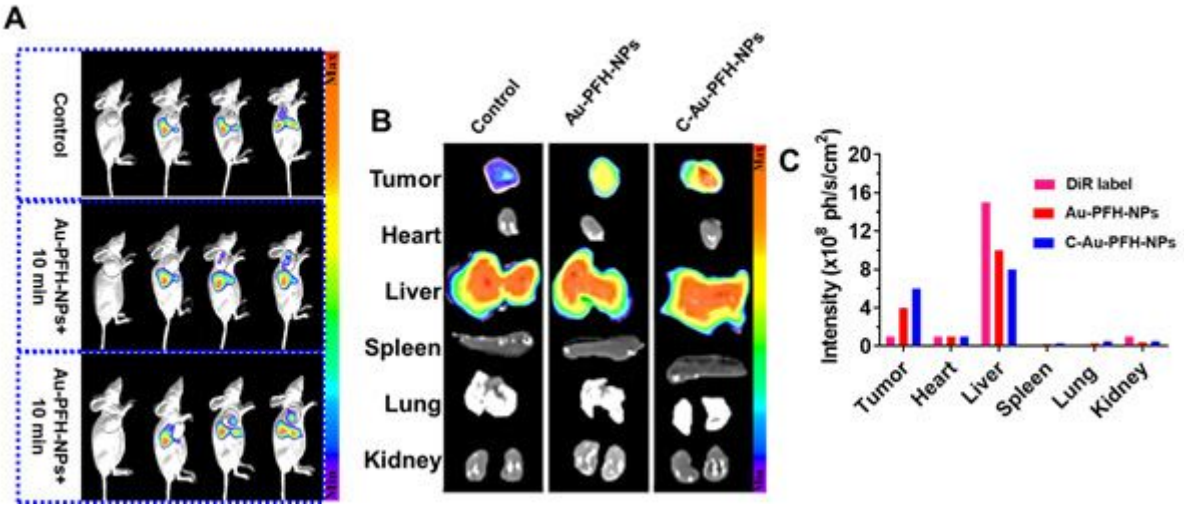

Figure 5

In vivo pharmacokinetics and biodistribution studies of Au-PFH-NPs and C-Au-PFH-NPs (A) In vivo plasma of the drugs following intravenous injection of Au-PFH-NPs and C-Au-PFH-NPs. (B)

Biodistribution studies of Au-PFH-NPs and C-Au-PFH-NPs. (C) The intensity of the DiR slabel Au-PFH-NPs and C-Au-PFH-NPs.

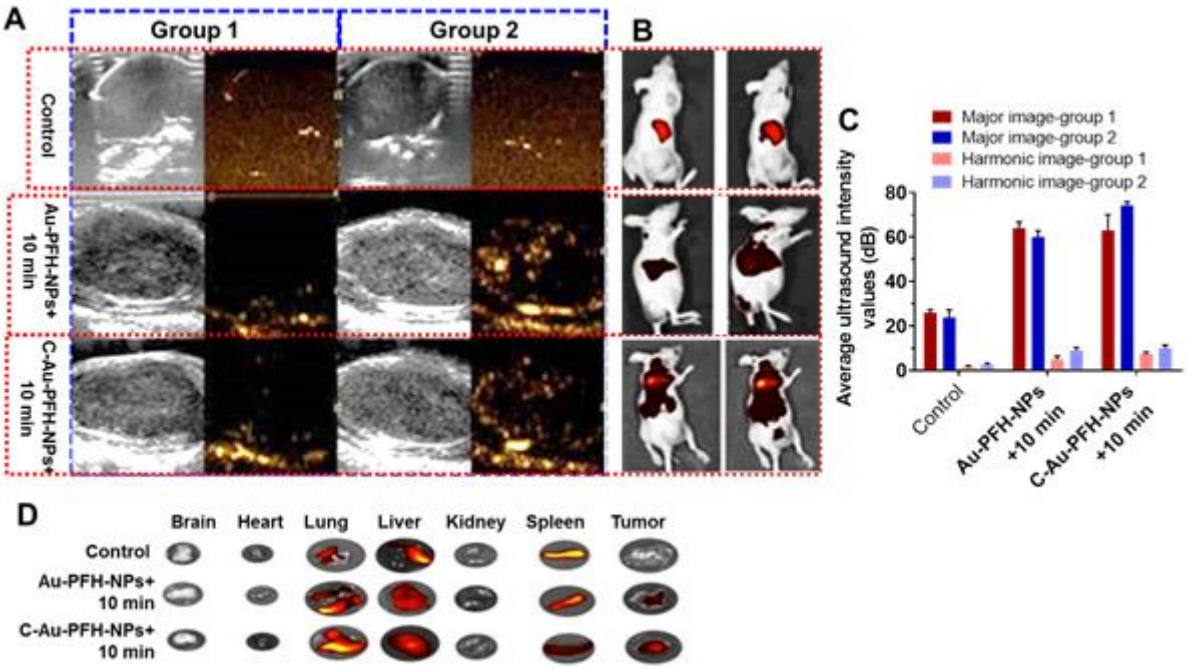

Figure 6

(A) Ultrapure sound image. (B) The organs used rats. (C) Average intensity values of Au-PFH-NPs and C-Au-PFH-NPs. (D) organs used ultrasound (Control-without ultrasound and Au-PFH-NPs and C-Au-PFH-NPs 10 min ultrasound exposure).

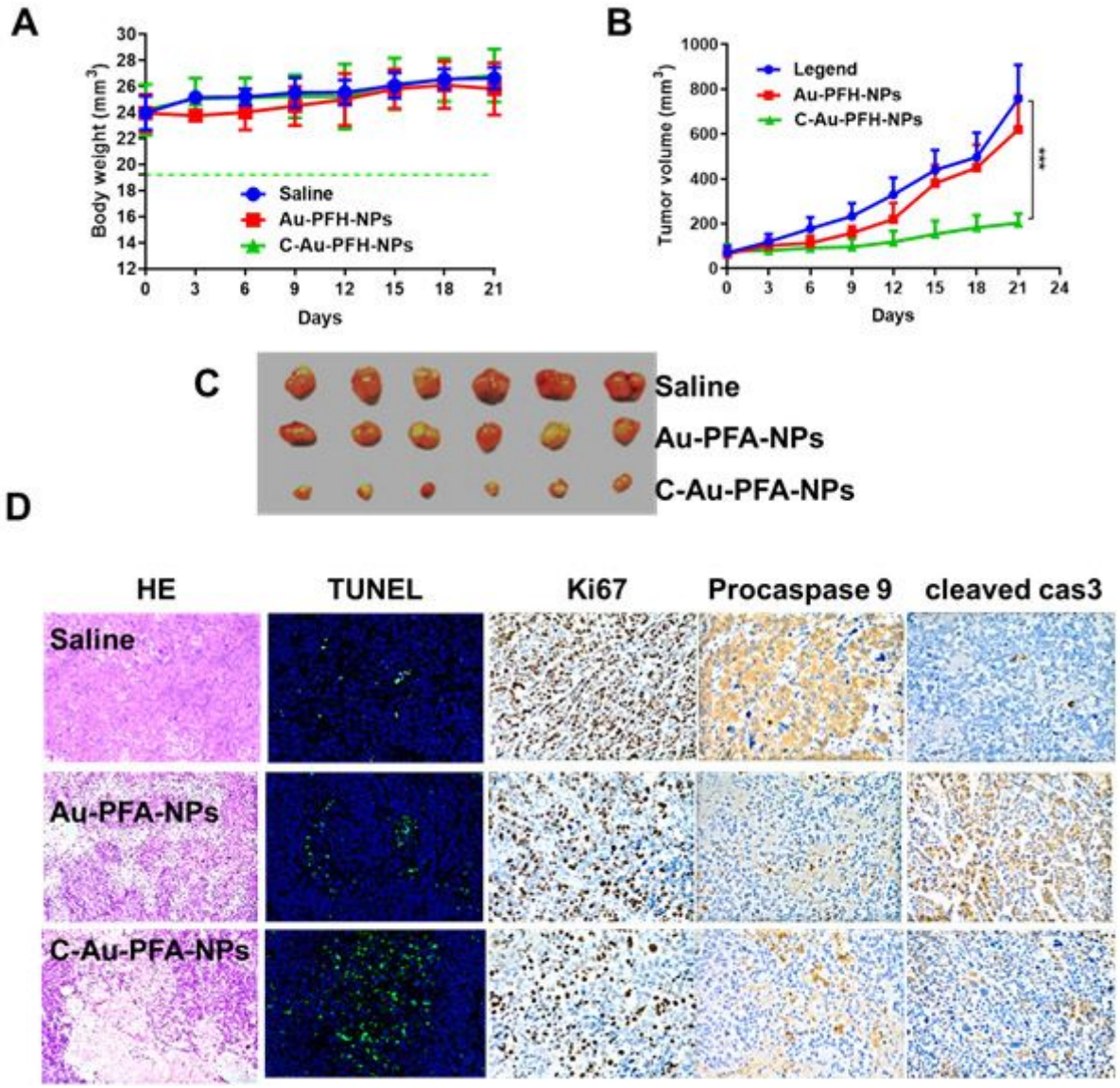

Figure 7

(A) Body weight and (B) tumor volume (mm3). (C) Morphology of the tumors 21 days after treatment. Tumor volume, tumor weight, and average body weight. (D) Representative HE, TUNEL, Ki67, procaspase, cleaved caspase three analysis of the excised tumors from the treated groups after injection of the drugs. (400x image magnification)

Supplementary Files

This is a list of supplementary files associated with this preprint. Click to download.

- Authorforms.docx